International Journal of Multiphase Flow 35 (2009) 219–226

Contents lists available at ScienceDirect

International Journal of Multiphase Flow

journal homepage: www.elsevier.com/locate/ijmulflow

A stochastic Langevin model of turbulent particle dispersion in the presence of thermophoresis

A. Dehbi *

Paul Scherrer Institut, Department of Nuclear Energy and Safety, Laboratory for Thermal-Hydraulics, 5232 Villigen PSI, Switzerland

ARTICLE INFO

Article history:
Received 28 March 2008
Received in revised form 18 September 2008
Accepted 24 November 2008
Available online 11 December 2008

ABSTRACT

Direct numerical simulation (DNS) and experimental data have shown that inertial particles exhibit concentration peaks in isothermal turbulent boundary layers, whereas tracer-like particles remain well mixed in the domain. It is therefore expected that the interactions between turbulence and thermophoresis will be strong in particle-laden flows where walls and carrier fluid are at significantly different temperatures. To capture turbulent particle dispersion with active thermophoresis, a coupled CFD-Lagrangian continuous random walk (CRW) model is developed. The model uses 3D mean flow velocities obtained from the Fluent 6.3 CFD code, to which are added turbulent fluid velocities derived from the normalized Langevin equation which accounts for turbulence inhomogeneities. The mean thermophoretic force is included as a body force on the particle following the Talbot formulation. Validation of the model is performed against recent integral thermophoretic deposition data in long pipes as well as the TUBA TT28 test with its detailed local deposition measurements. In all cases, the agreement with the data is very good. In separate parametric studies in a hypothetical cooled channel flow, it is found that turbulence strongly enhances thermophoretic deposition of particles with dimensionless relaxation times τ^+ of order 1 or more. On the other hand, the thermophoretic deposition of very small inertia particles ($\tau^+ < 0.2$) in the asymptotic region far from the injection point tends to that which characterizes stagnant flow conditions, in agreement with the DNS results of Thakurta et al.

1. Introduction

Thermophoresis is a mean force which drives particles down temperature gradients from hot to cold regions of the carrier fluid. Quantitative understanding of thermophoresis is of great practical interest in a multitude of areas, e.g. ceramic powder production in high temperature reactors, fouling and corrosion in heat exchangers and turbines, particle removal in thermal precipitators and automobile exhaust systems.

Considerable analytical efforts have been directed at understanding thermophoretic deposition in laminar pipe flows (Walker et al., 1979; Batchelor and Shen, 1985; Stratmann et al., 1988; Lin and Tsai, 2003l; Housiadas and Drossinos, 2005). The simple 1D formula by Housiadas and Drossinos (2005) was in particular found to be in good overall agreement with their more detailed 2D Lagrangian and Eulerian models as well as with the data by Montassier et al. (1991).

Investigations of thermophoretic phenomena in turbulent flow conditions have not in comparison been as numerous. Romay et al. (1998) conducted thermophoretic tests in turbulent pipe flows and deposition rates were deduced by subtracting the contribution of turbulent eddy impaction under isothermal conditions. In their accompanying model, the authors explicitly assumed that turbulent eddy impaction and thermophoretic contributions can be added up, i.e. that the two mechanisms are independent of one another. While clearly intended to render the problem tractable, the latter assumption is in general not accurate, as will be seen later, because turbulence strongly de-mixes inertial particles in inhomogeneous flows (Eaton and Fessler, 1994).

Housiadas and Drossinos (2005) developed a 2D Lagrangian non-stochastic model for turbulent thermophoretic deposition inside a pipe. The effect of the fluctuating fluid was modeled by adding the turbophoretic velocity (Reeks, 1983) in the particle equation of motion. Yet again, this formulation explicitly assumes that turbophoretic and thermophoretic contributions can be simply added up in the particle equations of motion. The model tended to overpredict turbulent thermophoretic deposition data of the TUBA TT28 test (Dumaz et al., 1993) and the Phebus FPT-0 test (Clément et al., 2003), particularly in the entrance region.

Kröger and Drossinos (2000) developed a discrete random walk model (DRW) for thermophoretic deposition in turbulent pipe. The model did not include a drift correction for the fluid velocity fluctuations, which may have produced the so-called "spurious drift" (MacInnes and Bracco, 1992), i.e. the non-physical accumulation

* Tel.: +41 56 310 27 11; fax: +41 56 310 27 99.
E-mail address: abdel.dehbi@psi.ch

0301-9322/$ - see front matter © 2008 Elsevier Ltd. All rights reserved.
doi:10.1016/j.ijmultiphaseflow.2008.11.006

of small inertia particles in the viscous sublayer. This eventually caused the over-prediction of thermophoretic deposition data.

Lo Iacono and Reynolds (2005) developed a Lagrangian stochastic model based on a continuous Markov process to describe the dispersion of Brownian particles in the presence of thermal gradients. Although the model was only concerned with Brownian particles, and could not be properly validated for flows with thermal gradients because of lack of data, it did demonstrate that stochastic models with correctly implemented physics can predict at least qualitatively the mechanisms governing turbulent particle dispersion.

Turbulent thermophoretic deposition in a channel flow was studied at a fundamental level using Direct Numerical Simulation (DNS) by Thakurta et al. (1998). The authors showed some interesting results, in particular that turbulence significantly increased particle deposition rates compared to the stagnant flow case for particles with dimensionless relaxation times of order 1 or above. This is directly attributable to the fact that turbulence causes concentration peaks of inertial particles inside the viscous sublayer (Marchioli and Soldati, 2002). This phenomenon of preferential particles build-up close to walls was also experimentally observed by Wang and Levy (2006) in isothermal flow past a flat plate.

The Langevin-based Continuous Random Walk (CRW) model is an attractive alternative to DNS/LES methods to describe turbulent fluid fluctuations seen by a particle. The CRW is capable of accurately describing the main features of turbulent particle dispersion in isothermal inhomogeneous flows as shown by e.g. Iliopoulos and Hanratty (1999), Mito and Hanratty (2002, 2004), Iliopoulos et al. (2003), Bockell and Loth (2006), and most recently Dehbi (2008). The main goal of this investigation is to extend the Langevin model to describe turbulent fluid velocity fluctuations in wall-bounded geometries when thermophoresis is active.

2. Particle force balance

A spherical particle is assumed to be entrained in a wall-bounded turbulent flow where thermal gradients are present. The only forces acting on the particle are taken to be drag, gravity and thermophoresis. Brownian diffusion is neglected since the simulated particles will have geometric diameters greater than 0.2 μm. The lift force is also ignored since it has very little impact on particles with dimensionless relaxation times less than 1 as shown by Slater et al. (2003). The vector force balance on a spherical particle is written as follows:

$$\frac{dU_p}{dt} = F_D(U - U_p) + g\left(1 - \frac{\rho_f}{\rho_p}\right) + F_{th} \tag{1}$$

where the drag force per unit mass may be expressed as:

$$F_D = \frac{18\mu}{\rho_p d_p^2} C_D \frac{Re_p}{24} \tag{2}$$

In the above, U is the fluid velocity, U_p is the particle velocity, ρ_p the particle density, ρ_f the fluid density, g the gravity acceleration vector, d_p the particle geometric diameter, μ the fluid molecular viscosity, and Re_p the particle Reynolds number defined as:

$$Re_p = \frac{d_p|U - U_p|}{\nu} \tag{3}$$

where ν being the fluid kinematic viscosity. The drag coefficient is computed in the Fluent CFD code (Fluent, 2006) from the following equation:

$$C_D = \beta_1 + \frac{\beta_2}{Re_p} + \frac{\beta_3}{Re_p^2} \tag{4}$$

where the βs are constants which apply to spherical particles for wide ranges of Re_p.

The thermophoretic force is computed following the formulation of the Talbot model (Talbot et al.,1980) since the latter is found to provide the best fit with a wide range of experimental data. Thus:

$$F_{th} = -D_{T,p}\frac{1}{m_p T}\nabla T \tag{5}$$

where T is the fluid temperature, m_p the particle mass and $D_{T,p}$ the thermophoretic coefficient defined as:

$$D_{T,p} = \frac{6\pi d_p \mu^2 C_s (k_f k_p + C_t Kn)}{\rho_f (1 + 3C_m Kn)(1 + 2k_f k_p + 2C_t Kn)} \tag{6}$$

where Kn is the particle Knudsen number, k_f and k_p, respectively the fluid and particle thermal conductivities, and C_s, C_t and C_m are dimensionless constants in the Talbot model having respective values of 1.17, 2.18 and 1.14.

The trajectory $x(x_1,x_2,x_3,t)$ of the particle is obtained by integration of the following velocity vector equation with respect to time:

$$U_p = \frac{dx}{dt} \tag{7}$$

In laminar flows, the expressions (1)–(7) are sufficient to compute the trajectory of individual particles. When turbulent fluctuations exist in the fluid flow, the computation of particle dispersion is no longer deterministic and the particle dispersion problem becomes more complicated to handle. To determine the mean dispersion statistics of particles, it is necessary to perform many trajectory computations. The stochastic modeling of the fluid velocity fluctuations is discussed in the next section. It will be assumed that only the fluctuations in the velocity field will influence particle motion. Fluctuations in the temperature will be ignored as second order effects, following the findings of Thakurta et al. (1998), as well as those of Kröger and Drossinos (2000).

3. The normalized Langevin equations

In the following section, we present the Langevin equations defining the fluctuating velocity field along a particle track. The domain is assumed to be wall-bounded, so that it can be subdivided in two regions: the boundary layer region with strongly anisotropic turbulence, and a bulk region where the turbulence is assumed approximately isotropic but generally inhomogeneous. Since the model is meant to handle both the boundary layer as well as the isotropic bulk regions, the Langevin equations will take different forms depending on the location of the particle.

3.1. The normalized Langevin equation in boundary layers

To improve the predictive abilities of the Langevin equation in boundary layers, Durbin (1983, 1984) and Thompson (1984), extending the ideas of Wilson et al. (1981), proposed that the Langevin equation be normalized to account for strongly inhomogeneous turbulence. Following Iliopoulos et al. (2003), the normalized Langevin equation in the boundary layer along the ith coordinate is written as:

$$d\left(\frac{u_i}{\sigma_i}\right) = -\left(\frac{u_i}{\sigma_i}\right)\cdot\frac{dt}{\tau_L} + d\eta_i + A_i dt \tag{8}$$

In the above, u_i is the fluid fluctuating velocity component, σ_i the rms of velocity $\sqrt{\overline{u_i^2}}$, τ_L a Lagrangian time scale, $d\eta_i$ a succession of uncorrelated random forcing terms, and A_i the mean drift correction term which ensures the well-mixed criterion (Thompson, 1987). Dehbi (2008) has shown that the normalized Langevin equa-

tions can be written as follows for the streamwise, normal, and spanwise directions of the boundary layer:

$$d\left(\frac{u_1}{\sigma_1}\right) = -\left(\frac{u_1}{\sigma_1}\right)\cdot\frac{dt}{\tau_L} + \sqrt{\frac{2}{\tau_L}}\cdot d\xi_1 \tag{9}$$

$$d\left(\frac{u_2}{\sigma_2}\right) = -\left(\frac{u_2}{\sigma_2}\right)\cdot\frac{dt}{\tau_L} + \sqrt{\frac{2}{\tau_L}}\cdot d\xi_2 + \frac{\partial\sigma_2}{\partial x_2}\cdot\frac{dt}{1+Stk} \tag{10}$$

$$d\left(\frac{u_3}{\sigma_3}\right) = -\left(\frac{u_3}{\sigma_3}\right)\cdot\frac{dt}{\tau_L} + \sqrt{\frac{2}{\tau_L}}\cdot d\xi_3 \tag{11}$$

where the $d\xi_i$s are Gaussian random numbers with zero mean and variance dt.

The Stokes number factor in the drift correction term of (10) is due to Bockell and Loth (2006). The particle Stokes number Stk is defined as:

$$Stk = \frac{\tau_p}{\tau_L} \tag{12}$$

where τ_p is the particle relaxation time defined according to the local particle Reynolds number:

$$\tau_p = \frac{C_c\rho_p d_p^2}{18\mu} \quad Re_p \le 1 \tag{13}$$

and :

$$\tau_p = \frac{4}{3}\frac{\rho_p}{\rho_f}\frac{C_c d_p^2}{C_D|U-U_p|} \quad Re_p > 1 \tag{14}$$

where C_c is the Cunningham correction slip factor which is nearly 1 for particles with diameters above 1 μm.

3.2. The normalized Langevin equation in the isotropic bulk

In the bulk region turbulence is taken to be isotropic, although not necessarily homogeneous. The Langevin equations become simpler in that region, and Dehbi (2008) showed that they can be expressed as:

$$d\left(\frac{u_1}{\sigma}\right) = -\left(\frac{u_1}{\sigma}\right)\cdot\frac{dt}{\tau_L} + \sqrt{\frac{2}{\tau_L}}\cdot d\xi_1 + \frac{1}{3\sigma}\cdot\frac{\partial k}{\partial x_1}\cdot\frac{dt}{1+Stk} \tag{15}$$

$$d\left(\frac{u_2}{\sigma}\right) = -\left(\frac{u_2}{\sigma}\right)\cdot\frac{dt}{\tau_L} + \sqrt{\frac{2}{\tau_L}}\cdot d\xi_2 + \frac{1}{3\sigma}\cdot\frac{\partial k}{\partial x_2}\cdot\frac{dt}{1+Stk} \tag{16}$$

$$d\left(\frac{u_3}{\sigma}\right) = -\left(\frac{u_3}{\sigma}\right)\cdot\frac{dt}{\tau_L} + \sqrt{\frac{2}{\tau_L}}\cdot d\xi_3 + \frac{1}{3\sigma}\cdot\frac{\partial k}{\partial x_3}\cdot\frac{dt}{1+Stk} \tag{17}$$

where σ is the rms of the isotropic velocity field, and k the turbulent kinetic energy.

4. Solution methods

Eqs. 9, 10, 11 and 15, 16, 17 describe possible changes along a particle path of the turbulent fluid velocities in the boundary layer and bulk region, respectively. The integration of these equations in time is done using the first order implicit Euler method, and the time step is taken to be min (10^{-6} s, $0.1\tau_p$), which was shown to be small enough not to influence the results. The integration of the Langevin equations necessitates Eulerian statistics to close the problem. The Eulerian rms of velocity are obtained from DNS fits of channel flow (Re = 13,000) as given by Dreeben and Pope (1997), while the Lagrangian timescales are obtained from fits given by Kallio and Reeks (1989). The reader is referred to Dehbi (2008) for more details.

While the integration of the Langevin equations in the bulk region poses no particular problem in 3D geometries, care must be exercised when the particle is in the boundary layer, because one must correctly assign the Eulerian rms values in a local body-fitted coordinates system which varies with particle location. The algorithm to do so is explained at length by Dehbi (2008). Property variations with temperature are taken into account by the CFD code. However, it is necessary to make some assumptions concerning the Eulerian statistics fits which are obtained in isothermal conditions. It will thus be assumed that the Eulerian velocity statistics hold for a viscosity which is evaluated at the mean temperature between the bulk fluid and the wall.

5. Results and discussion

In this section, the model predictions are compared to various thermophoretic deposition tests conducted in turbulent pipe flows. Additional simulations are subsequently conducted in a hypothetical channel with fully developed flow to study more in depth different parameters affecting deposition rates, paralleling the DNS investigations of Thakurta et al. (1998). For all the simulations, the CFD Best Practice Guidelines (ERCOFTAC, 2000) were followed to ensure that the flow field results were grid-independent. In all cases the boundary layer was fully resolved with about 30 mesh points.

In addition, since the geometries are simple, the k–ε model for turbulence is chosen for the CFD mean flow modeling. Owing to the low velocities encountered in the simulations, the "incompressible-ideal-gas law" option is used to model density variations with temperature and the viscosity is computed following the Sutherland formulation. In Lagrangian particle tracking exercises, the particle sample was such that halving its size would not change the deposited fraction by more than 1%. In addition, a particle is deemed "trapped" when its center of mass is located less than one particle radius from the wall. Finally, in the specification of particle inertia, the dimensionless relaxation time τ^+ is defined as:

$$\tau^+ = \frac{\tau_p u^{*2}}{\nu} \tag{18}$$

where u^* is the friction velocity and ν is the kinematic viscosity.

5.1. Pipe flow simulations

Validation of the model against experimental data is done in this section. Three investigations have been chosen for this purpose. The first one by Dumaz et al. (1993) features local information on the deposition rate, while the other two by Tsai et al. (2004) and Romay et al. (1998) provide integral data on the deposition rate. While the Tsai tests were conducted with very low inertia particles, Romay et al. used particles with non-negligible inertia in which the interplay between thermophoresis and turbophoresis is expected to be quite important.

5.1.1. The TUBA TT28 test

The TUBA tests (Dumaz et al., 1993) were conducted to validate thermophoretic deposition models used in nuclear safety computer codes. The cooled test section consisted of a 1 m long tube, with inner diameter 0.018 m. In test TT28 conducted in turbulent conditions, the gas was heated up to 641 K, and the wall was kept at 312 K. The carrier gas was air flowing at a rate of 1.95 g/s under atmospheric pressure, which translated into an inlet velocity of 14.1 m/s. The Reynolds number based on the inlet conditions is 4300. The aerosol used in these tests is CsI (density 5000 kg/m^3, thermal conductivity 1.1 W/(m K) and specific heat capacity 200 J/(kg.K)) with an Aerodynamic Mass Median Diameter (AMMD) of 1.19 μm. The dimensionless relaxation time of the particles is 0.12, per equation (18), meaning that the particles could be considered to be nearly tracers in the absence of thermophoresis.

The local particle deposition profile was carefully measured in 13 sections comprising the test section. In addition to the test section proper, a 0.5 m adiabatic conditioning length upstream of the cold wall is modeled to provide a developing section for the flow. The finest CFD grid consists of 2.2 million hexahedral meshes. After the fluid flow solution is converged, 10,000 monodisperse particles are injected uniformly at the entrance face of the conditioning section and tracked using the CFD-Langevin model until they hit the wall or leave the domain. Simulations were also conducted by turning off the fluid fluctuating velocities, which is subsequently referred to as the "mean flow model" or MFM.

The results showing the cumulative deposition fraction along the pipe length are displayed in Fig. 1. The stochastic Langevin model captures very well both the trends and the magnitudes of deposition. On the other hand, the MFM widely overpredicts deposition, particularly near the entrance of the cooled pipe. The MFM gives predictions similar to what Housiadas and Drossinos (2005) obtained with their 2D non-stochastic Lagrangian model. This stresses then that the non-inclusion of radial fluid fluctuations exaggerates the thermophoretic deposition rates of very small inertia particles.

5.1.2. The Tsai et al. tests

Tsai et al. (2004) conducted thermophoretic deposition tests in a turbulent pipe flow with air as the carrier gas. The test section was a pipe of total length 2.74 m and inner diameter 0.0043 m. The first length of 1.56 m served as a conditioning section to heat the carrier gas up from room temperature to 343 or 398 K, depending on the tests. The test section measured 1.18 m and its wall was cooled and kept at a constant temperature of 296 K. The carrier gas had a flow rate of 20 or 32 L/min (based on room temperature), corresponding to *Re* of 6580 and 10,200, respectively. Monodisperse NaCl particles (density 2160 kg/m^3, thermal conductivity 6.0 W/(m K), and specific heat capacity 835 J/(kg K)) with geometric diameters between 0.04 and 0.5 μm were used. Only one series of tests, i.e. *Re* = 6580, was conducted with both charged and neutral particles. The other series used particles with Boltzmann equilibrium charge. The authors found a marked increase in deposition when particles having Boltzmann equilibrium charge are used instead of neutral particles. Given that we do not consider the electrostatic force in this investigation, we will restrict ourselves to the comparison of the model with the neutral test series (Tsai, 2007). In addition, we consider only tests conducted with particles larger than 0.2 μm, since below that level, Brownian diffusion – which is not modeled here – becomes important. The dimensionless relaxation time τ^+ for the largest test particles is 0.24, i.e. the particles would behave like tracers if the conditions were isothermal.

The finest CFD grid used had 4.1 million hexahedral cells. Once the mean flow solution converges, 10,000 particles are injected at the entrance face of the conditioning section and their trajectories subsequently followed. The predicted integral deposition is compared with the data in Fig. 2. As can be seen, the Langevin model predictions are in quite good agreement with the data. Simulations were also conducted by turning off the fluid fluctuating velocities (MFM), and in this case particles were uniformly injected at the entrance of the cooled test section. The MFM widely overpredicts the deposition data, as in the simulation of the TUBA TT28 test (Dumaz et al., 1993).

5.1.3. The Romay et al. tests

Romay et al. (1998) performed thermophoretic deposition tests in pipe flow at turbulent conditions (*Re* of 5517 and 9656). The pipe has a diameter of 0.0049 m, a conditioning length of 0.94 m in which the fluid was heated up, and a cooling test section of length 0.965 m which was kept at 293 K. The aerosol consisted of monodisperse NaCl particles with geometric diameters between 0.1 and 0.7 μm. Given the flow conditions, the dimensionless relaxation times τ^+ are as high as 0.75, which can result in non-negligible particle accumulation near the wall. The authors extracted the thermophoretic deposition from the total deposited fraction assuming eddy impaction and thermophoretic mechanisms are decoupled. To obtain the eddy impaction contribution, the authors conducted isothermal tests which provided dimensionless deposition velocities V^+ as a function of τ^+. The authors then compared this thermophoretic deposition data with their simple model based on the Talbot correlation (Talbot et al., 1980) and the significant assumption that the particle concentration remains uniform across the flow area. The authors found that their model consistently underpredicted the inferred thermophoretic deposition data by as much as a factor of 2, and the discrepancy was higher as the particle relaxation time and driving temperature difference increased. The authors attributed the discrepancy to factors not addressed in their simple model such as enhancement due to eddy impaction and non-uniform particle concentrations. The latter two effects are in fact directly related since turbulence causes inertial particles to accumulate in the viscous sublayer, from which point they can be more effectively transported to the walls by thermophoresis.

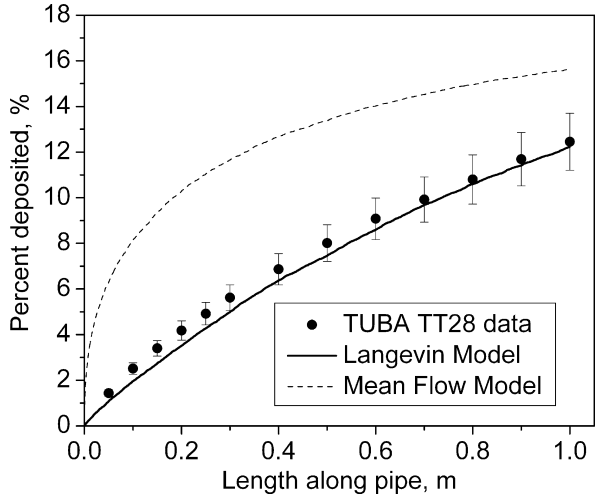

Fig. 1. Model predictions compared to data from the TUBA TT28 test.

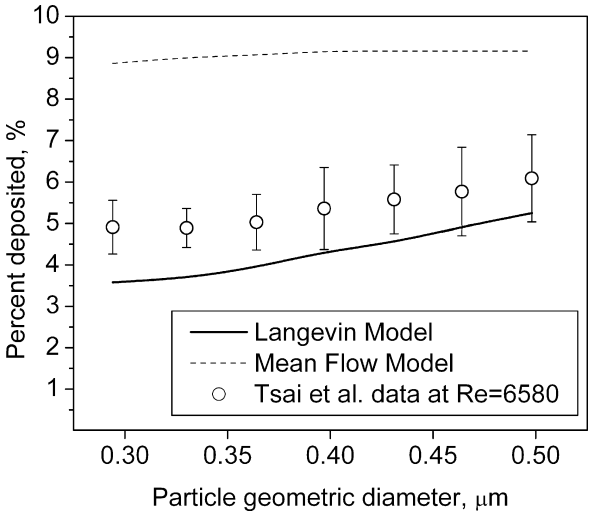

Fig. 2. Model predictions compared to data from the test by Tsai et al. at *Re* = 6580.

It should be mentioned that the isothermal deposition velocities by Romay et al. (1998) were about a factor 10 larger than those predicted by the Liu–Agarwal correlation (1974). This enhanced deposition can be attributed to surface roughness effects, or residual charge. As mentioned earlier, Tsai et al. (2004) experimentally showed that even a slight charging can account for a sizable deposition when compared to neutral particles. The present model does not account for charge or wall surface roughness effects, and therefore it cannot directly simulate the Romay et al. (1998) tests in their raw data format. However, if one assumes the spurious surface roughness and charge effects are effectively filtered out by the computational procedure outlined by Romay et al. (1998), then a comparison between the Langevin model and the inferred thermophoretic deposition data becomes possible. To keep the number of computations reasonable, only the tests with the highest inlet temperature, i.e. 415 K, are simulated. These tests accounted for the greatest discrepancy between the authors' simple model and their data.

The CFD mesh consists of 0.66 million hexahedral cells and particle tracking is performed with 10,000 monodisperse particles injected uniformly from the entrance of the cooled section. Table 1 shows the comparison between integral deposition fraction and predictions of various models. The Romay model and the MFM provide roughly the same predictions for the particle deposited fraction, which is not surprising because both models assume uniform particle concentration and no radial fluid fluctuations. Both models underpredict the data, especially for higher inertia particles. The Romay model actually predicts a lower deposition as τ^+ increases, which contradicts the experimental trend. On the other hand, the Langevin model agrees well with the data, and correctly predicts higher deposition for larger particles.

5.2. Simulation of particle deposition in a parallel channel

To understand more deeply how turbulence affects thermophoretic deposition, sensitivity studies are conducted in a hypothetical horizontal parallel channel geometry with height H of 0.01 m, length 0.8 m, and width (span) 0.1 m. The air flow enters the section with a temperature of 600 K. The CFD grid is made of 1.0 million hexahedral meshes.

The wall is cooled in such a way that the heat flux is maintained at 8000 W/m^2, so that the thermophoretic deposition velocity at the wall for a given particle size is nearly constant throughout the domain. The average flow parameters for the channel section where particles are tracked are indicated in Table 2. The flow parameters do not change much in the domain so that this simulation is conceptually similar to the "periodic channel" conditions of the DNS by Thakurta et al. (1998), and the MFM here is the counterpart of the "stagnant gas model" in that investigation. Table 3 gives the diameters of the simulated particles and their corresponding dimensionless relaxation times. Based on the channel height and mean temperature, the Reynolds number is 7220, which is quite comparable to the values encountered in the preceding pipe flow cases. The flow conditions are such that the channel has a height of about 430 in dimensionless units. Thus the computational volume is roughly evenly split between the boundary layer ($y^+ < 100$) and the bulk region.

Table 2
Mean parameters in the parallel channel particle tracking section.

Inlet section mean velocity (m/s)	28.3
Mean friction velocity (m/s)	1.70
Injection point bulk gas temperature (K)	581.2
Outlet bulk gas temperature (K)	537.4
Injection point wall temperature (K)	487.2
Outlet wall temperature (K)	444.4
Mean fluid temperature (K)	512.6
Mean fluid density (kg/m^3)	0.694
Mean kinematic viscosity (m^2/s)	39.2×10^{-6}
Reynolds number	7220

Table 3
Particle diameters and their respective dimensionless relaxation times.

d_p (μm)	τ^+
0.44	0.05
0.98	0.20
1.62	0.50
2.35	1.0
4.16	3.0
5.41	5.0
7.70	10.0

Particles are injected uniformly along a line joining the two walls in the middle of the span at a distance of 30H downstream of the channel inlet, hence ensuring fully developed flow at the point of injection. Particle dispersion is thus studied in the remaining 50 channel heights. The deposition velocity is computed over the last 20H, far enough from the injection point.

5.2.1. Effect of turbulence on particle concentrations

The effect of particle inertia on concentration profiles is studied in this section in order to better understand the interactions between turbulence and thermophoresis. Four classes of particles having relaxation times τ^+ of 0.05, 1, 5, and 10 are considered. In each simulation, 100,000 unit density particles are injected uniformly and subsequently tracked as they disperse. At an instant t corresponding to the mean time required by a fluid particle to travel a distance of 40H (i.e. 80% of the distance between the injection and the outlet planes), the tracks are frozen, and the volumetric particle distribution profile is determined. To do so, the volume of the channel is subdivided in N_b wall parallel bins along the height of the channel. The bins are thinner near the wall and become progressively wider as one moves towards the center of the channel, according to the following formula for the bth bin thickness:

$$\Delta y_b^+ = \frac{Re_\tau}{2}\left(1 - \cos\left(\pi \cdot \frac{b-1}{N_b - 1}\right)\right) \tag{19}$$

where the Reynolds number based on the friction velocity is 430, and N_b is 51. The purpose of such grading is to resolve well the laminar and buffer layers near le wall (y^+ of 30), in which the thermophoretic force is the strongest. To compute the particle concentration profile, one simply counts the airborne particles in each bin, and then normalizes this number with the volume of the bin as well as the total number of particles. The normalized particle concentra-

Table 1
Deposition fraction (%) of different models versus the experimental data by Romay et al.

Particle diameter (μm)	τ^+	Romay et al. model	CFD mean flow model	CFD Langevin model	Romay et al. data
0.300	0.18	0.105	0.105	0.120	0.155 ± 0.030
0.482	0.39	0.100	0.109	0.159	0.170 ± 0.015
0.700	0.75	0.090	0.109	0.200	0.185 ± 0.020

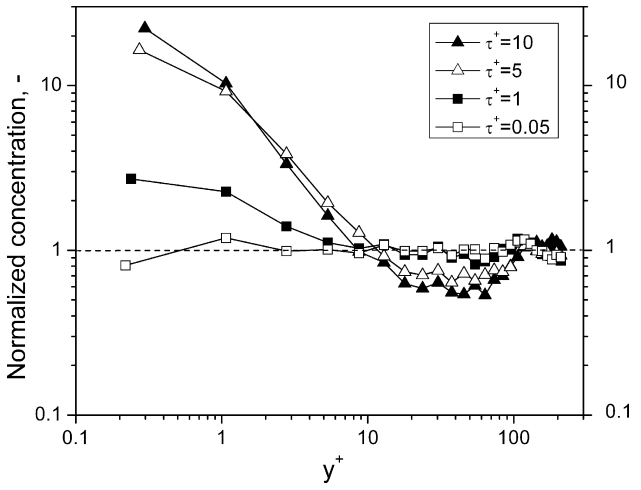

Fig. 3. Normalized concentration profiles for different particle inertias.

tion is shown in Fig. 3. One sees that particles with the lowest inertia ($\tau^+ = 0.05$), remain approximately well mixed in the channel except in the region $y^+ < 1$ where the concentration becomes smaller due to depletion caused by thermophoretic deposition. As particle inertia increases, ever larger concentration peaks develop well inside the laminar sublayer. This is quite consistent with many DNS studies (e.g. Eaton and Fessler,1994; Thakurta et al., 1998; Marchioli et al., 2007). These profiles explain a great deal of the findings reported in the next sections.

A comparison of the normalized concentration profiles is provided for particles with τ^+ of 5 for the case where thermophoresis is not activated. These particles have low deposition velocities in isothermal conditions, but are inertial enough to build up large concentration peaks close to the wall, and hence their deposition rate is significantly increased when thermophoresis is turned on. As seen in Fig. 4, thermophoresis reduces the concentration peak while beyond the laminar sublayer ($y^+ > 5$), the concentration profiles for the two cases are essentially identical. Both findings are in agreement with the DNS results of Thakurta et al. (1998) for particles of similar inertia (τ^+ of 3.99).

5.2.2. The effect of inertia on deposition rates in the asymptotic region

We concentrate thereafter on the asymptotic region in order to compute deposition rates that could be conceptually comparable to those of the "periodic channel" DNS investigations by Thakurta et al. (1998). We compute hence the deposition velocities in the region between 60*H* and 80*H*. Three models are compared: (1) Langevin model with active thermophoresis, (2) Langevin model with no thermophoresis and (3) Mean Flow Model (MFM).

Again, particles are injected uniformly from the vertical line joining the parallel channels starting from $L = 30H$. 10,000 particles is a large enough sample to get stationary statistics for the deposition in models (1) and (3). For model (2), a 100,000 sample was necessary for particles with $\tau^+ \geqslant 3.0$, and no attempt was made to compute the deposition velocities for particles with $\tau^+ < 3.0$ because an unreasonably high computational effort would be required owing to the very low deposition rates.

The deposition velocity is defined as:

$$V^+ = \frac{1}{2}\frac{H}{L}\frac{U}{u^*}\ln\left(\frac{C_{in}}{C_{out}}\right) \tag{20}$$

In the above, U is the mean velocity, L the length of the channel section where deposition is studied, and C_{in} and C_{out} refer to the particle number concentrations entering and leaving the section, respectively.

The deposition velocities versus τ^+ are shown in Fig. 5. When both turbulence and thermophoresis are active, the deposition rate increases very significantly as τ^+ increases beyond 1. This is due to the near-wall particle preferential accumulation which becomes stronger with particle inertia. Once particles reach the laminar sublayer, they are efficiently transported to the wall by the thermophoretic force which is highest in that region. As particle inertia becomes smaller ($\tau^+ < 0.2$), the deposition rate of the Langevin model tends to values predicted by the MFM. The thermophoretic force causes the largest enhancement in deposition rates for the intermediate inertia particles which accumulate near the wall but which cannot penetrate past the laminar sublayer, not having gathered a large enough velocity to do so. When thermophoresis is active, these accumulated particles are very effectively pushed to the wall. The latter results are all in quantitative agreement with the DNS results by Thakurta et al. (1998). The magnitudes of the deposition velocity between this study and the one by Thakurta et al. (1998) cannot however be directly compared, because the latter study was performed with friction velocities 4 times higher than the present study, and with about twice the temperature differential.

5.2.3. Impact velocity spectra

Following Thakurta et al. (1998), we examine in this section the velocity with which particles hit the wall when both thermophore-

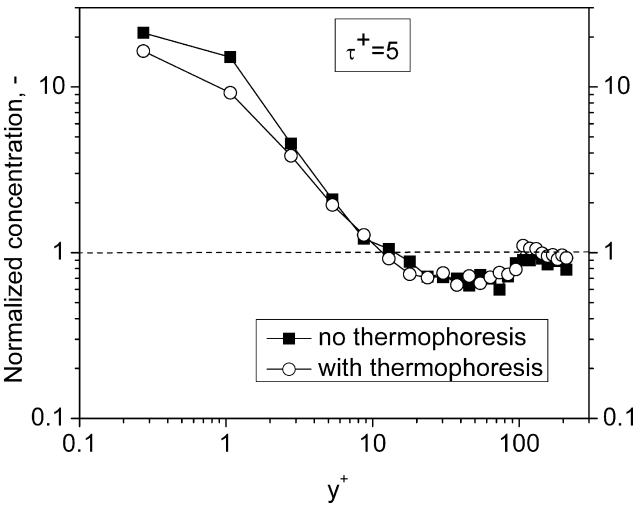

Fig. 4. Normalized concentration profiles with and without thermophoresis for $\tau^+ = 5$.

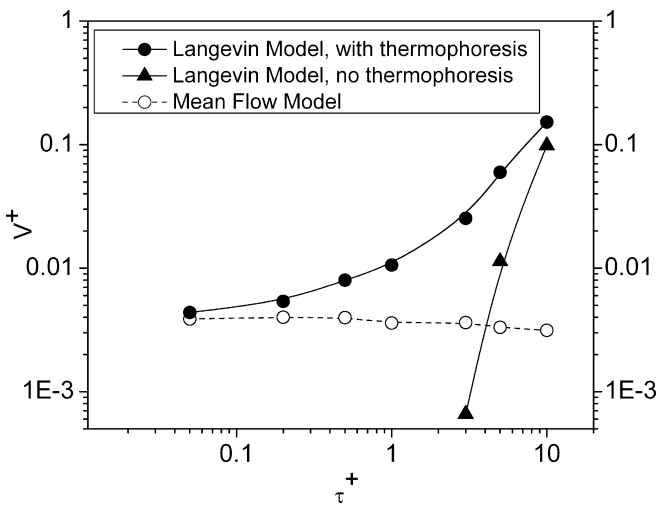

Fig. 5. Comparison of deposition rates for the Langevin model (with and without thermophoresis) and the MFM.

sis and turbulence are activated. We consider particles with relaxation times 1, 5, and 10, representing low, intermediate, and high inertia particles, respectively. Figs. 6–8 show histograms giving the spectrum of the impact velocity V^+_{imp}, which is the wall normal component of velocity upon inelastic particle collision with the wall, normalized with the friction velocity.

The spectrum of the $\tau^+ = 1$ particles is very sharp with a peak at 99.4%. The impact velocity is identical to the thermophoretic deposition velocity in the MFM. This indicates that thermophoresis is the only mechanism responsible for deposition of these low inertia particles. This would obviously be the case for particles with lower relaxation times. For intermediate inertia particles with $\tau^+ = 5$, the peak is at 89.9%, pointing to the fact that thermophoresis is still the main deposition mechanism, but a non-negligible fraction of particles deposit with higher velocities, showing the growing importance of eddy impaction. For high inertia particles with $\tau^+ = 10$, only 48.3% of deposition can be attributed to thermophoresis. Roughly half the particles deposit by eddy impaction, including some "free flight" impacts which have velocities up to three orders of magnitude greater than the thermophoretic velocity. These findings are in agreement with the DNS results by Thakurta et al. (1998).

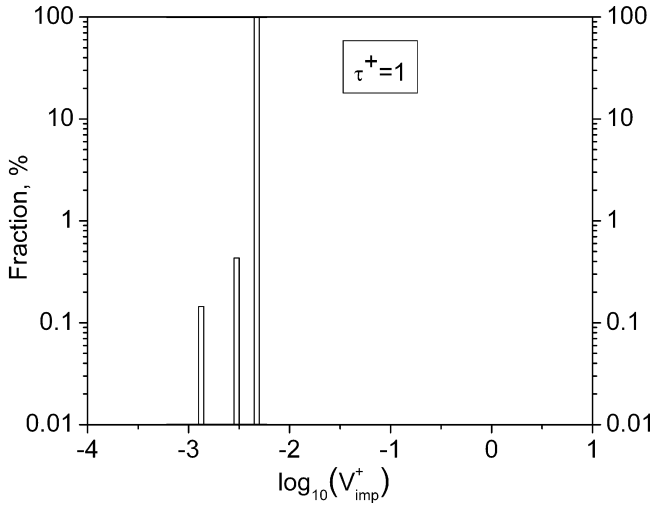

Fig. 6. Histogram of impact velocity for $\tau^+ = 1$.

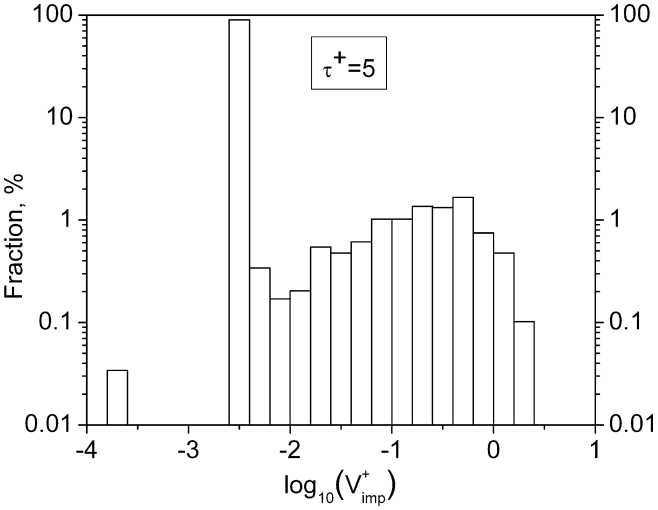

Fig. 7. Histogram of impact velocity for $\tau^+ = 5$.

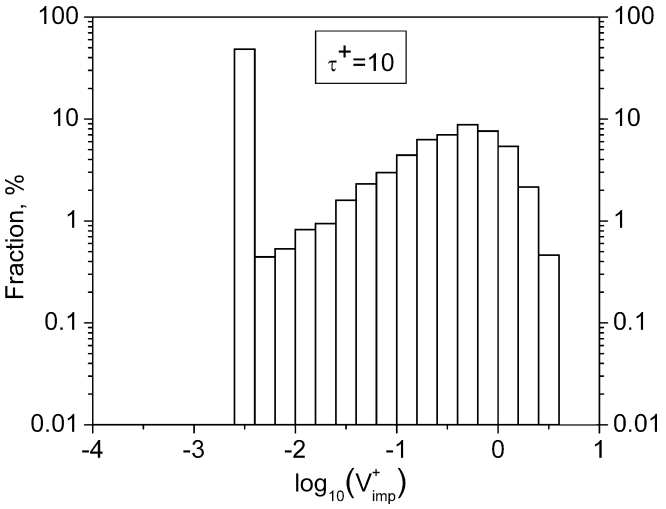

Fig. 8. Histogram of impact velocity for $\tau^+ = 10$.

6. Conclusions

To properly capture turbulent particle dispersion in wall bounded flows with active thermophoresis, a Lagrangian continuous random walk (CRW) model is developed. The model makes use of mean flow velocities obtained from the CFD code Fluent, whereas the fluctuating velocities are based on the normalized Langevin equation which includes recent improvements to handle particles with arbitrary inertia. The mean thermophoretic force is added as a body force on the particle and follows the formulation by Talbot et al. (1980). A comprehensive validation and simulation exercise is performed from which the following conclusions can be drawn:

- The model agrees well with recent integral thermophoretic deposition data in long pipes (Romay et al. 1998; Tsai et al., 2004) as well as the TUBA TT28 test (Dumaz et al, 1993) with its detailed local deposition measurements.
- In the asymptotic region where the deposition rate is approximately constant, turbulence greatly enhances particle deposition rates as τ^+ increases beyond 1. For τ^+ of order 0.2 or less, the deposition rate tends to the value characterizing stagnant flow conditions. These results agree well with the DNS findings of Thakurta et al. (1998) in a periodic channel flow.
- It is generally incorrect to assume that turbulent eddy deposition and thermophoresis can be decoupled and their respective deposition rates simply added up. For small and intermediate inertia particles ($0.2 < \tau^+ < 5$), the two mechanisms actually work in tandem, such that turbulence causes particles to accumulate in the laminar sublayer, and thermophoresis acts to push them towards the wall. It is only for high inertia particles ($\tau^+ \geqslant 5$) that eddy impaction and thermophoresis compete with each other. This is apparent in the impact velocity spectra which show sharp peaks centered about the thermophoretic deposition velocity for particles with $\tau^+ < 5$, but which display ever broader distributions as τ^+ increases beyond 5.

Acknowledgments

The author wishes to express his gratitude to Professor Chuen-Jinn Tsai of the National Chiao Tung University (Taiwan) for providing his unpublished data on neutral particle deposition, and to

Professor Mike Reeks of the University of Newcastle (UK) for useful discussions.

References

Batchelor, G.K., Shen, C., 1985. Thermophoretic deposition of particles in gas flowing over cold surfaces. J. Colloid Interface Sci. 107, 21–37.

Bockell, T.L., Loth, E., 2006. Stochastic modeling of particle diffusion in a turbulent boundary layer. Int. J. Multiphase Flow 32, 1234–1253.

Clément, B., Hanniet-Girault, N., Repetto, G., Jacquemain, D., Jones, A.V., Kissane, M.P., on der Hardt, P., 2003. LWR severe accident simulation: synthesis of the results and interpretation of the first Phebus FP experiment FPT0. Nucl. Eng. Des. 226, 5–82.

Dehbi, A., 2008. Turbulent particle dispersion in arbitrary wall-bounded geometries: a coupled CFD-Langevin-equation based approach. Int. J. Multiphase Flow 34, 819–828.

Dreeben, T.D., Pope, S.B., 1997. Probability density function and Reynolds-stress modeling of near-wall turbulent flows. Phys. Fluids 9, 154–163.

Dumaz, P., Drossinos, Y., Capitao, J. Areia, Drosik, I., 1993. Fission product deposition and revaporization phenomena in scenarios of large temperature differences. In: ANS Proceedings 1993 National Heat Transfer Conference, American Nuclear Society, Atlanta, GA, pp. 348–358.

Durbin, P.A., 1983. Stochastic differential equations and turbulent dispersion. NASA Reference Publication 1103.

Durbin, P.A., 1984. Comments on the papers by Wilson et al. (1981) and Legg and Raupach (1982). Bound. Layer Meteorol. 29, 409–411.

Eaton, J.K., Fessler, J.R., 1994. Preferential concentration of particles by turbulence. Int. J. Multiphase Flow 20, 169–209.

ERCOFTAC, 2000. European Research Community on Flow Turbulence and Combustion (ERCOFTAC) Best Practice Guidelines, Version 1.

Fluent, 2006. Fluent 6.3: Users Guide, Lebanon, USA.

Housiadas, C., Drossinos, Y., 2005. Thermophoretic deposition in tube flow. Aerosol Sci. Technol. 39, 304–318.

Iliopoulos, I., Hanratty, T.J., 1999. Turbulent dispersion in a non-homogeneous field. J. Fluid Mech. 293, 45–71.

Iliopoulos, I., Mito, Y., Hanratty, T.J., 2003. A stochastic model for solid particle dispersion in a nonhomogeneous turbulent field. Int. J. Multiphase Flow 29, 375–394.

Kallio, G.A., Reeks, M.W., 1989. A numerical simulation of particle deposition in turbulent boundary layers. Int. J. Multiphase Flow 3, 433–446.

Kröger, C., Drossinos, Y., 2000. A random-walk simulation of thermophoretic particle deposition in a turbulent boundary layer. Int. J. Multiphase Flow 26, 1325–1350.

Lin, J.-S., Tsai, C.-J., 2003. Thermophoretic deposition efficiency in a cylindrical tube taking into account developing flow at the entrance region. J. Aerosol Sci. 34, 569–583.

Liu, B.Y.H., Agarwal, J.K., 1974. Experimental observation of aerosol deposition in turbulent flow. Aerosol Sci. 5, 145–155.

Lo Iacono, G., Reynolds, A.M., 2005. A Lagrangian stochastic model for the dispersion and deposition of Brownian particles in the presence of a temperature gradient. J. Aerosol Sci. 36, 1238–1250.

MacInnes, J.M., Bracco, F.V., 1992. Stochastic particle dispersion modeling and the tracer particle limit. Phys. Fluids A 4, 2809–2824.

Marchioli, C., Soldati, A., 2002. Mechanisms for particle transfer and segregation in turbulent boundary layer. J. Fluid Mech. 468, 283–315.

Marchioli, C., Picciotto, M., Soldati, A., 2007. Influence of gravity and lift on particle velocity statistics and transfer rates in turbulent vertical channel flow. Int. J. Multiphase Flow 33, 227–251.

Mito, Y., Hanratty, T.J., 2002. Use of a modified Langevin equation to describe turbulent dispersion of fluid particles in a channel flow. Flow Turbul. Combust. 68, 1–26.

Mito, Y., Hanratty, T.J., 2004. A stochastic description of wall sources in a turbulent field. Part 2. Calculation for a simplified model of horizontal annular flows. Int. J. Multiphase Flow 30, 803–825.

Montassier, N., Boulaud, D., Renoux, A., 1991. Experimental study of thermophoretic particle deposition in laminar tube flow. J. Aerosol Sci. 22, 677–687.

Reeks, M.W., 1983. The transport of discrete particles in inhomogeneous turbulence. J. Aerosol Sci. 14, 729–739.

Romay, F.J., Takagaki, S.S., Pui, D.Y.H., Liu, B.Y.H., 1998. Thermophoretic deposition of aerosol particles in turbulent pipe flow. J. Aerosol Sci. 29, 943–959.

Slater, S.A., Leeming, A.D., Young, J.B., 2003. Particle deposition from two-dimensional turbulent gas flows. Int. J. Multiphase Flow 29, 721–750.

Stratmann, F., Fissan, H., Papperger, A., Friedlander, S., 1988. Suppression of particle deposition to surfaces by the thermophoretic force. Aerosol Sci. Technol. 9, 115–121.

Talbot, L., Cheng, R., Schefer, R., Willis, D., 1980. Thermophoresis of particles in a heated boundary layer. J. Fluid Mech. 101, 737–758.

Thakurta, D.G., Chen, M., McLaughlin, J.B., Kontomaris, K., 1998. Thermophoretic deposition of small particles in a direct numerical simulation of turbulent channel flow. Int. J. Heat Mass Transfer 41, 4167–4182.

Thompson, D.J., 1984. Random walk modeling of dispersion in inhomogeneous turbulence. Q. J. Roy. Meteorol. Soc. 110, 1107–1120.

Thompson, D.J., 1987. Criteria for the selection of stochastic models of particle trajectories in turbulent flows. J. Fluid Mech. 180, 529–559.

Tsai, C.-J., 2007. Private communication.

Tsai, C.-J., Lin, J.-S., Aggarwal, S., Chen, D.-R., 2004. Thermophoretic deposition of particles in laminar and turbulent tube flows. Aerosol Sci. Technol. 38, 131–139.

Walker, K.L., Homsy, G.M., Geyling, R.T., 1979. Thermophoretic deposition of small particles in laminar tube flow. J. Colloid Interface Sci. 69, 138–147.

Wang, J., Levy, E.K., 2006. Particle behavior in the turbulent boundary layer of a dilute gas-particle flow past a flat plate. Exp. Therm. Fluid Sci. 30, 473–483.

Wilson, J.D., Thurtell, G.W., Kidd, G.E., 1981. Numerical simulation of particle trajectories in inhomogeneous turbulence. Part 2. Systems with variable turbulent velocity scale. Bound. Layer Meteorol. 21, 423–441.